Eur Spine J (2006) 15: 299–307
DOI 10.1007/s00586-005-0935-1

ORIGINAL ARTICLE

Marc-Antoine Rousseau
David S. Bradford
Tamer M. Hadi
Kirk L. Pedersen
Jeffery C. Lotz

The instant axis of rotation influences facet forces at L5/S1 during flexion/extension and lateral bending

Received: 23 December 2003
Revised: 29 March 2005
Accepted: 12 April 2005
Published online: 20 September 2005

M.-A. Rousseau · D. S. Bradford
T. M. Hadi · K. L. Pedersen
J. C. Lotz (✉)
Orthopaedic Bioengineering Laboratory,
Department of Orthopaedic Surgery,
University of California, San Francisco,
533 Parnassus Ave, San Francisco,
CA, 94143
E-mail: jlotz@itsa.ucsf.edu
Tel.: +1-415-4767881
Fax: +1-415-4761128

Abstract Because the disc and facets work together to constrain spinal kinematics, changes in the instant axis of rotation associated with disc degeneration or disc replacement may adversely influence risk for facet overloading and arthritis. The relationships between L5/S1 segmental kinematics and facet forces are not well defined, since previous studies have separated investigations of spinal motion and facet force. The goal of this cadaveric biomechanical study was to report and correlate a measure of intervertebral kinematics (the centrode, or the path of the instant axis of rotation) and the facet forces at the L5/S1 motion segment while under a physiologic combination of compression and anterior shear loading. Twelve fresh-frozen human cadaveric L5/S1 joints (age range 50–64 years) were tested biomechanically under semi-constrained conditions by applying compression plus shear forces in several postures: neutral, and 3° and 6° of flexion, extension and lateral bending. The experimental boundary conditions imposed compression and shear representative of in vivo conditions during upright stance. The 3-D instantaneous axis of rotation (IAR) was calculated between two consecutive postures. The facet joint force was simultaneously measured using thin-film sensors placed between both facet surfaces. Variations of IAR location and facet force during motion were analyzed. During flexion and extension, the IAR was oriented laterally. The IAR intersection with the mid-sagittal plane moved cephalad relative to S1 endplate during flexion ($P=0.010$), and posterior during extension ($P=0.001$). The facet force did not correlate with posture ($P=0.844$). However, changes in the facet force between postures did correlate with IAR position: higher IAR's during flexion correlated with lower facet forces and vice versa ($P=0.04$). During lateral bending, the IAR was oblique relative to the main plane of motion and translated parallel to S1 endplate, toward the side of the bending. Overall, the facet force was increased on the ipsilateral side of bending ($P=0.002$). The IAR positions demonstrate that the L5 vertebral body primarily rotates forward during flexion (IAR close to vertebral body center) and rotates/translates backward during extension (IAR at or below the L5/S1 intervertebral disc). In lateral bending, the IAR obliquity demonstrated coupling with axial torsion due to resistance of the ipsilateral facet.

Keywords Human · Lumbosacral joint · Spine biomechanics · Instantaneous axis of rotation · Facet force

Introduction

Degenerative disc disease is an important public health problem with multiple dimensions: personal, social, and professional. It is well recognized that facet arthritis is associated with disc degeneration, and this is typically attributed to loss of disc height and consequently increased posterior column loads. However, in addition to disc height loss, intervertebral kinematics becomes progressively erratic with increasing disc degeneration, being characterized by significant variability in the instantaneous axis of rotation (IAR) position (centrode) [9]. Since spinal movement is constrained by both the disc and facet joints, disc material property deterioration with degeneration must influence facet forces [16]. Unfortunately, the influence IAR position fluctuations on facet loads, and consequently arthritis risk, has not been investigated.

Recently, advances in surgical technique and instrumentation have generated interest in disc arthroplasty as a novel method for treating degenerative disc disease. Different intervertebral implant designs have been used for restoring disc height and painless motion [37]. As with disc degeneration, disc replacement alters the disc/facet synergy in yet, unknown ways. Consequently, the influence of many implant design choices, such as the degree of constraint, bearing surface shape, and size, may alter facet forces and the patients risk for developing facet arthritis.

Because of its caudal location and its crucial role in spine sagittal balance, the L5/S1 joint is one of the most commonly degenerated levels and the most common site of disc replacement for degenerative disc disease [3, 15, 18]. Due to the sagittal obliquity of the sacral endplate, anterior intervertebral shear is significant at this level [2, 11, 19]. Consequently, the facet joints are critical for preventing spondylolisthesis and constraining inter-segmental motion.

Several authors have described aspects of L5/S1 kinematics in vivo [28, 29] and in vitro under different loading conditions [19, 23, 25, 30, 41, 42]. Others have reported the force transmitted through the facet joints in various intervertebral positions under pure axial compression [7, 32, 35]. These previous in vivo studies were limited by not measuring facet forces, while in vitro studies were limited by simplified loading conditions, since in addition to compression, the L5/S1 level supports significant anterior shear [3, 19, 25]. Given that the disc is viscoelastic and spinal kinematics can vary with the magnitude and nature of superimposed loading, previous studies may have missed clinically-relevant interactions between the kinematics and facet forces. The goal of the study was to simultaneously measure spinal kinematics and facet forces during motion in a human cadaveric model of the healthy L5/S1 joint under physiologic compression and shear.

Methods

Specimen selection and preparation

The lumbosacral spine was harvested from 12 human donors aged 50–64 at the time of death (8 male and 4 female). Only specimens with no radiographic evidence of bone disease or joint degeneration (osteophytes, disc space narrowing, facet hyperthrophy) were used in this study. Specimen preparation consisted in meticulous removal of muscular tissue so as to retain the integrity of the capsular and ligamentous elements. For each specimen, the superior half of the L5 vertebrae and inferior half of S1 vertebrae were potted in polymethylmetacrylate (PMMA), so that S1 end-plate was parallel to the PMMA surface and clamping faces.

Experimental device

Each specimen was placed in a servo-hydraulic apparatus (Bionix 858, MTS Systems Corp. Eden Meadow, MN, USA) such that the disc was oriented at 40° relative to the horizontal axis (Fig. 1). This angle was chosen to reflect the average 39° sacral slope in standing position [14, 38]. The specimens were loaded with an 850 N vertical force applied via a frictionless surface (polished steel lubricated with machine oil). This force was chosen to match estimates for L5/S1 in the standing position based on disc pressure [21] and myo-electric [33] measurements, and therefore represents both gravity and muscular loading. The 850 N vertical force generated

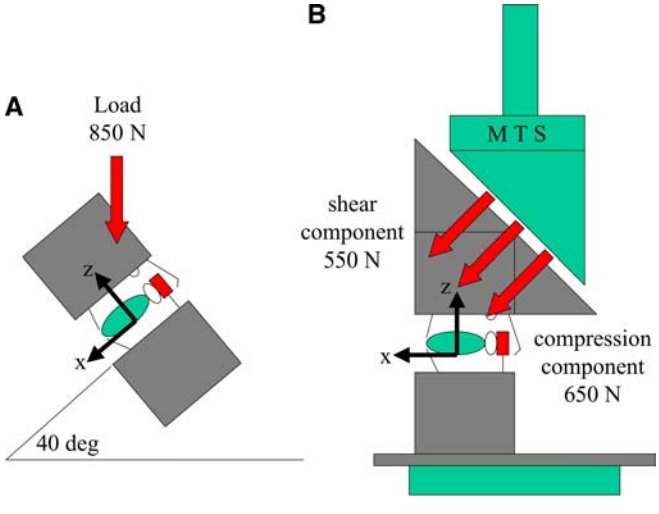

Fig. 1 Schematic diagram of L5/ S1: 40° sacral slope and 850 N load in standing position (**a**). Testing device constrained L5 posture in flexion, extension, and bending for investigating L5/S1 kinematics (**b**). Load is uniformly distributed and applies both shear and compression. Axial torsion was unconstrained

650 N of disc compression and 550 N of horizontal shear consistent with free body analyses of L5/S1 [2, 19, 39] based on specific morphometric studies [8, 20]. The semi-constrained feature of the testing apparatus is such that the location of the resultant force at the frictionless surface varies, and thereby minimizes its distance to the IAR. Consequently, confounding moments about the IAR are minimized [6]. In addition, at the start of each experiment, the rotational actuator of the test system was used to adjust the axial rotation position of the frictionless surface so as to minimize differences in bilateral facet forces. This adjustment procedure accounted for any slight misalignment of the L5/S1 specimens within the PMMA.

Wedges were added at the frictionless interface to impose 3° and 6° flexion/extension and lateral bending postures. The 12° total range of motion in the sagittal and the frontal plane was below the normal physiological zone of the L5/S1 joint [25]. Automatic coupled torsions [23, 25] were allowed in the oblique frictionless plane. Each 3° rotation between two consecutive postures defined a 'motion sector'.

Specimen preconditioning [39] consisted in ten cycles of complete loading and unloading in neutral posture over 5 min. During testing, data were collected after 2 min of loading for each posture. Tissues were kept moist during testing by wrapping in saline-soaked gauze.

Outcome measures

Instantaneous axis of rotation

For a rigid body in three-dimensional (3-D) space, the motion from one position to another can be described by the sum of a rotation around a single axis and a translation (perpendicular to the plane of rotation) along this axis. For that general case, the axis is called the helicoidal axis [39]. For small displacements, movement occurs around an 'instantaneous axis.' For a null translation along the axis, the instantaneous helicoidal axis is called IAR. All necessary information to calculate the instantaneous helicoidal axis are contained in the transformation matrix, which is a mathematical description of the rigid-body movement from one position to another, and includes a square 3×3 rotation matrix and a 3×1 translation matrix. Consequently, the helicoidal axis is just an alternate representation of the transformation matrix.

We calculated the transformation matrix using the method of Kinzel [13], based on 3-D coordinates of four non-coplanar landmarks placed on the moving vertebra (L5). Then the direction and the position and of the axis was determined in the 3-D space according to the method of Spoor and Velpaus [36]. Finally these data were transformed to a local coordinate frame based on the radiographic anatomy. The origin of the orthogonal right-handed frame was the center of the endplate of S1, the *X*-axis being sagittal, the *Y*-axis coronal, and the *Z*-axis vertical and perpendicular to the endplate (Fig. 1). IAR direction was described using the inclination (*I*; angle between the axis and the horizontal plane that is equivalent to a latitude from the S1 endplate) and the declination (*D*; angle between the axis and the sagittal plane that is equivalent to a longitude). IAR position was described as the position of the unique point, P (x_p, y_p, z_p), of the axis so that the distance OP is the shortest distance from the origin (O) to the axis (P). Therefore, OP is perpendicular to the IAR.

Using the direct linear transformation method, three Falcon strobe cameras, utilizing Eva 6.0 software (Motion Analysis Corp. Santa Rosa, CA, USA) established the 3-D coordinates of four reflective markers placed on L5, and of one reflective marker a fixed on S1 for each posture of L5. The transformation matrix and IAR between consecutive postures of L5 were computed using the average of 300 repeated measures of the position of each marker collected at each posture. The marker on S1 was also visible on specimen radiograph for matching the IAR to the specific anatomy of each specimen.

Despite the precision of the strobe cameras for determining the markers coordinates (±0.25 mm), random error was propagated and magnified by the algorithm of matrix computation. Woltring [40] assessed that the error in IAR position was inversely proportional to the amount of rotation: random error tends towards infinity when rotation tends towards zero. Other factors like the marker distance to the real IAR, and the radius of distribution of the markers, also can contribute to the error magnitude. We utilized a standard door hinge oriented in a pre-defined direction to determine the accuracy of our experimental set up in the IAR calculation. Based on a pilot study using this approach we estimated our absolute error for IAR placement during pure rotation, 3° movements as 4 mm, and IAR direction as 1°.

Facet force

Simultaneous to the IAR calculation, the compression force transmitted through the left and right facet joints was recorded using thin pressure sensors (Flexiforce A101–500, Tekscan Inc, South Boston, MA, USA). These were introduced into the right and left joint space through a vertical cut in the joint capsule. The sensors were 10 mm in diameter, 0.2 mm thick, and made of flexible mylar and contain ink whose resistance varies linearly to the applied force. Sensor output was recorded at 5 Hz and averaged using data acquisition software (Labview 6.1, National Instruments, Austin, TX, USA).

We calibrated our sensor by applying pre-determined forces via contact surfaces of different areas and demonstrated that the output voltage varied linearly with the force regardless of the pressure area. The calibration ratio was 500 N/V (±5%).

For a given rotation, we hypothesized that the facet force variation (difference in facet force between adjacent postures, δF) would be proportional to the distance (d) between IAR and facet joint,

$$\delta F \propto d \tag{1}$$

However, the force sensor introduced in the joint records only the force component perpendicular to the joint surface (δm). If α is the angle between the sensor surface and δF (Fig. 2a), then

$$\delta m = \delta F . \sin \alpha \tag{2}$$

By combining Eqs. 1 and 2, one gets,

$$\delta m \propto d . \sin \alpha \tag{3}$$

As the facet joint space is considered vertical (orthogonal to the superior S1 endplate), α corresponds to the angle between the endplate and the line between the facet joint and the IAR. Then

$$d . \sin \alpha = h \tag{4}$$

where h is the IAR height relative to the facet joint level.

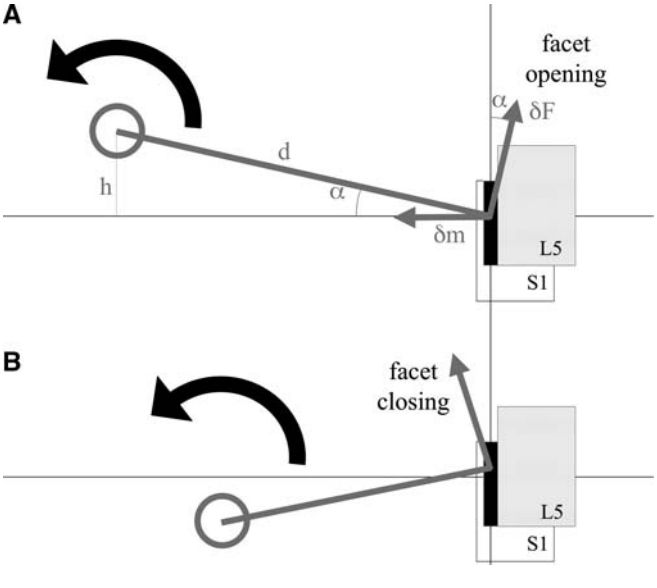

Fig. 2 Schematic of a lateral view of L5/S1 facets. Facet force variation (δF) in the facet joints in flexion/extension is related to height (h) of the IAR assuming that L5/S1 facets are perpendicular to S1 endplate (**a**). Facets open into flexion when the IAR is above the facet level. Facets close into flexion when the IAR is below the facet level (**b**)

Consequently, from Eqs. 3 and 4 it is apparent that the facet force is proportional to the IAR height,

$$\delta m \propto h \tag{5}$$

To test this hypothesis, we compared changes in the facet force measurement between adjacent postures (δm) to the calculated IAR height for those adjacent postures (h).

Statistics

All statistical analyses were performed using SPSS statistical software (Version 11.5, SPSS Inc., Chicago, IL, USA). Standard analysis of variance (ANOVA) procedures were used to compare group means and to estimate the effect of the specimen variables (parent specimen, motion sector, and direction of motion, entered as categorical variables) on the measured parameters of interest (IAR position and direction, and facet force, entered as continuous variables). When appropriate ($P < 0.05$), LSD post hoc tests were performed to identify group subsets with significant differences. Left and right facet forces were combined so that they were considered repeated measures within the same specimen in flexion/extension. In lateral bending, they were combined relative to the bending direction.

Since the facet force was measured with a single sensor that is 10 mm in diameter, we could not distinguish the specific location of the contact force within that zone. We, therefore, compared the facet force variation (δm) for those postures where the IAR was above the facet sensor zone to those postures where the IAR was below the facet sensor zone using one way ANOVA.

Results

Facet force data from three out of 24 joints were erratic (due to a broken sensor) and determined to be unreliable and therefore were removed from the calculations.

Flexion/extension

In flexion/extension, the IAR direction was similar for every motion sector. The average inclination was 1.3° ($P = 0.37$) and the average declination was 91.4° ($P = 0.701$). The IAR was therefore considered perpendicular to the main plane of motion, and its position was described as its intersection with the mid-sagittal plane ($y_i = 0$, Fig. 3a, Table 1

The x-coordinate of the IAR intersection with the midsagittal plane (x_i) was significantly different between motion sectors ($P = 0.001$). Post-hoc tests showed that

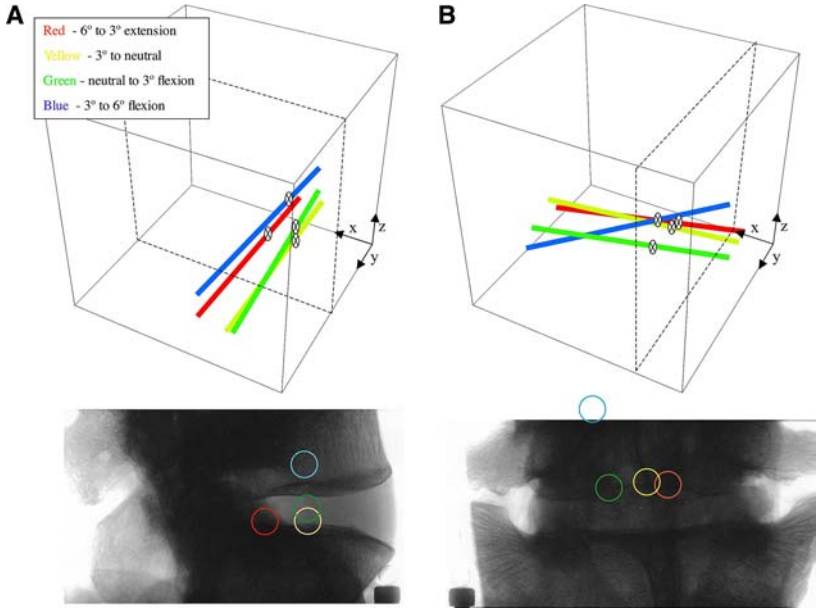

Fig. 3 Example of IAR data. Three-dimensional representation of the IAR in flexion/extension (**a**) and lateral bending (**b**). Intersections of the IAR and the sagittal and the coronal plane through the center of the disc are represented on a lateral and an AP radiograph respectively. The diameter of the circles corresponds to the average error in position (4 mm). The circle color code (red/yellow/green/blue) represents differing positions from extension to flexion and from left to right lateral bending (see legend)

the IAR was more posterior for the motion sector between 3° and 6° extension than for all other sectors. The z-coordinate of the IAR intersection with the midsagittal plane (z_i) was significantly different between motion sectors ($P = 0.010$). Post-hoc tests showed that the IAR was significantly higher between 3° and 6° flexion than for all other sectors.

The facet force did not vary consistently with posture during flexion/extension ($P = 0.844$; Table 2). However, during flexion movements, the facet force variation (δm) was significantly less when the IAR was above the facet sensor zone as compared to when it was below this zone ($P = 0.04$; Fig. 4). The average transmitted force through each facet for all specimens was 49.5 N.

Lateral bending

In lateral bending, the IAR declination was 1.8° and similar for every motion sector ($P = 0.565$). The IAR inclination varied with the motion sector ($P = 0.011$); post hoc test demonstrated that it was significantly higher after 3° in left lateral bending, and changed in right lateral bending. Because of the IAR obliquity, the IAR position was described in the general case as the position of P (Table 3). The x-coordinate of the IAR position (x_p) varied with the sector of motion ($P = 0.002$). Post hoc test showed that the IAR was more posterior beyond 3° bending in both directions. The y-coordinate of IAR position (y_p) varied significantly according the sector of motion during lateral bending ($P < 0.001$). Post-hoc tests showed that the IAR moved horizontally towards the bending beyond 3° bending in both directions. The z-coordinate (z_p) varied between sectors of motion ($P = 0.036$). Post hoc tests showed that the IAR was higher beyond 3° lateral bending in both directions.

The facet force was related to the posture ($P = 0.002$) in lateral bending and increased to the side of the bending. Post-hoc tests demonstrated that facet force increased significantly in the first 3° lateral bending (Table 4).

Table 1 Direction (inclination and declination) and coordinates of the IAR intersection with the midsagittal plane in flexion/extension (x_i, y_i, z_i)

Flexion/extension					
Motion sector	Inclination (°)	Declination (°)	x_i (mm)	y_i (mm)	z_i (mm)
3–6 ° extension	2.2 ± 0.9	91.6 ± 1.1	−12.3 ± 1.7	0	4.6 ± 3.1
0–3 ° extension	1.7 ± 0.8	90.6 ± 1.0	−8.8 ± 1.3	0	6.7 ± 1.3
0–3 ° flexion	0.3 ± 0.8	92.0 ± 0.9	−6.8 ± 1.2	0	5.7 ± 1.7
3–6 ° flexion	1.0 ± 0.7	91.6 ± 0.8	−7.3 ± 0.9[a] *	0	13.5 ± 2.2[a] *

[a] Significant variation: the IAR moved up in flexion and backward in extension
Values are given as Averages ± standard error

Table 2 Facet force in flexion/extension

Flexion/etension	
Posture	Average facet force (N)
6° extension	54.1 ± 14.6
3° extension	51.6 ± 12.6
Neutral	50.4 ± 9.8
3° flexion	47.6 ± 10.6
6° flexion	43.9 ± 9.0

Values are given as Averages ± standard error

Discussion

The goal of this study was to investigate relationships between intervertebral kinematics and facet forces during physiologic motion and loading of L5/S1. We observed that the IAR was normally located in the posterior part of the intervertebral disc, and moved superiorly during flexion, posteriorly during extension, and ipsilaterally during lateral bending. As expected, coupled axial rotation was associated with lateral bending. While the facet force did not show a uniform variation in flexion/extension because of interspecimen variability, it was correlated with the horizontal IAR displacement in lateral bending, such that the facet force increased in the ipsilateral facet.

Our observation that the IAR was perpendicular to the sagittal plane in flexion/extension and located at the posterior part of the intervertebral disc is consistent with prior reports based on planar measurements in vitro [9, 12] and in vivo [22, 31, 43] using the graphical method of Reulaux. The Reulaux method calculates the instantaneous center of rotation by drawing bisectors between landmarks on successive radiographs or photographs. This 2D method is less accurate compared to the 3D approach used in the current study [24, 27], which may explain why our observation that the IAR moves superiorly, perpendicular to S1 endplate during flexion, and posteriorly, parallel to the endplate during extension, has not been described previously [9, 22, 43].

The IAR path relative to S1 endplate demonstrates that from extension to flexion, L5 primarily translates anteriorly at first (i.e., the IAR is low during motion between 6° and 0° degrees of extension), and subsequently rotates forward when at the flexion limit (since the IAR approaches the geometric center of L5 during motion between 3° and 6° of flexion). This motion in flexion/extension reflects posture-varying roles of the disc and facet joints in constraining movement, and is consistent with reports that the facet contact area moves upwards into flexion [7].

We noted significant interspecimen variability in the facet force trend with posture that is contrary to the classical notion that facet forces systematically increase into extension [1, 4, 7, 35]. This discrepancy may in part be due to different loading conditions—prior studies were conducted using either pure moments or axial compression while we utilized compression plus anterior shear. Additionally, our data are the first to demonstrate a significant vertical IAR movement relative to S1 endplate. This vertical movement may explain facet force variation during sagittal motion, since the facet joint space theoretically opens or closes depending on whether the IAR is above or below the level of the joint (Fig. 2). That is, if the facet joint spaces are considered vertical (i.e., perpendicular to the endplate of S1), the IAR height and facet force should be linearly related during flexion/extension. Therefore, our experimental data (Fig. 4) support the hypothesis that the IAR height

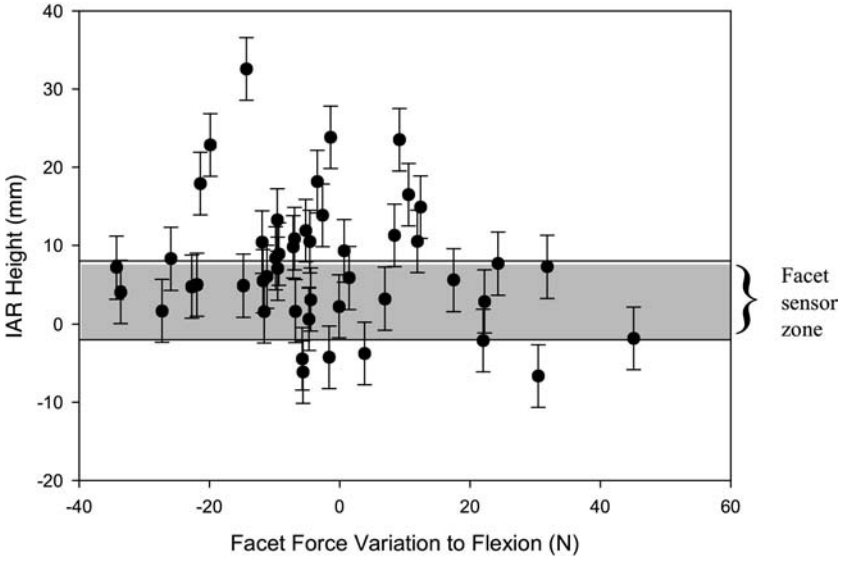

Fig. 4 IAR distance to S1 endplate (z_i: mm) plotted against facet force variation (N) for each 3° rotation into flexion. The "gray zone" corresponds to the facet height and hence force sensor location. The average facet force variation between two consecutive postures during flexion was −4.8 N when the IAR was located above the force sensor, and +7.2 N when the IAR was located below the force sensor ($P = 0.040$). The IAR height is related to the facet force variation in flexion/extension

Table 3 Direction (inclination an declination) and coordinates of the IAR position in lateral bending (x_p, y_p, z_p)

Lateral bending					
Motion sector	Inclination (°)	Declination (°)	x_p(mm)	y_p(mm)	z_p (mm)
3–6 ° left	21.0 ± 6.4	1.6 ± 0.4	−11.2 ± 1.3	−6.7 ± 1.2	19.2 ± 1.6
0–3 ° left	17.7 ± 5.2	1.4 ± 0.3	−6.7 ± 1.5	−1.1 ±1.0	13.9 ± 2.3
0–3 ° right	27.0 ± 2.8	2.1 ± 0.4	−9.6 ± 2.2	−2.0 ± 2.1	15.8 ± 2.6
3–6 ° right	33.3 ± 2.5 *	2.1 ± 0.4	−13.9 ± 2.1[a] *	−9.7 ± 1.6[a] *	20.8 ± 2.8[a] *

[a] Significant variation: the IAR moves up backward and in the bending direction in lateral bending ; inclination increases beyond 3° lateral bending

determines whether the facets open or close during sagittal plane movements (Fig. 2).

Our lateral bending data revealed IAR 3-D obliquity, which is due to coupling between lateral bending and axial rotation. That is, if lateral bending were not associated with axial rotation, then the IAR direction would have been perpendicular to the plane of bending. Since bending was applied by simulating the 40° sacral obliquity (Fig. 1), the expected IAR inclination would have been 40°. Rather, the actual average IAR inclination was 28.2°, with the 11.8° difference due to induced coupled rotation perpendicular to the main plane of motion. By decomposing the moment relative to the main plane of motion and its perpendicular plane (the frictionless surface in the testing device), our data demonstrates that the coupling was so that right bending of L5 was coupled with right axial rotation and vice versa. This result, under semi-constrained shear and compression in the oblique lumbo-sacral joint, is consistent with the observation of others when documenting coupled rotations of L5/S1 under pure moment loading conditions in vitro [5, 26] and in vivo [29].

Horizontal IAR displacement to the side of the bending is contrary to previous reports of using 2-D data [39]. This may be due to 3-D coupled motion as a confounding factor in previous 2-D methods. Our interpretation of the simultaneous horizontal IAR pathway and facet force increase to the side of the motion (significant Pearson correlation, $P = 0.015$) is that the ipsilateral facet blocks L5 lateral translation in bending. The IAR inclination increases and posterior displacement beyond 3° bending confirm that the impingement of the ipsilateral facet leads to coupling between lateral bending and axial torsion.

Table 4 Facet force in lateral bending. Averages ± standard error

Lateral bending	
Posture	Average facet force (N)
−6°	20.7 ± 6.7
−3°	22.0 ± 4.5
Neutral	36.9 ± 5.8
3°	68.2 ± 15.9
6°	58.4 ± 16.1[a] *

Values are given as Averages ± standard error
[a] Significant increase in the facet force ipsilaterally to the bending between neutral and 3° bending

Our results are potentially limited by our testing boundary conditions that allowed four degrees of freedom for L5 (compression, AP translation, lateral translation, and axial torsion). Two degrees of freedom were constrained (sagittal and frontal rotation). The fact that the testing device was semi-constrained may have led to asymmetry in facets impingement, because of the inevitable slight misalignment of the specimen in the apparatus. Facet asymmetry may have introduced artifacts in the kinematic or facet data, in spite of the rotational pre-adjustment of the apparatus. However, the current methodology provides a major advantage by utilizing a uniform and controlled load on the superior vertebra that results in physiologic combinations of compression plus shear. As the IAR is unknown before testing and mobile during motion, other loading conditions that use a fixed axis force would have theoretically generated variable and unknown moments around the IAR [6], leading to uncertain boundary conditions and uncertain results.

Another limitation is the precision of the overall assessment of the IAR. As mentioned in the Methods Section, algorithm and instrumentation factors limited the IAR precision to ±/−4 mm for 3° of movement. Consequently, IAR movements less than this limit could not be detected reliably. Yet, despite this and inevitable specimen-to-specimen variability, we noted several statistically significant trends in IAR position and facet force.

Finally, this study was also limited by the circular area of the force sensor that was about half the size of the facet joint surface. This mismatch created the potential that the facet contact area moved beyond measurement area during testing. However, the relatively continuous nature of the facet force measurements between postures suggested that this was not the case.

Also, a vertical cut in the facet joint capsule was necessary for inserting the sensors during preparation. This did not appear to adversely affect segmental kinematics as has been reported by others using pressure Fujifilm paper for mapping facet forces [7, 17].

Conclusions

Despite these potential limitations, our results demonstrate consistent relationships between IAR location and facet forces. These relationships highlight the interaction between the intervertebral disc and posterior elements for both load support and kinematics constraint. We anticipate that the awareness of the specific location of the IAR during motion and its influence on facet joints will be important for understanding the initiation of facet arthritis. For example, since it has been suggested that erratic IAR locations are associated with degenerative disc disease [10, 34], our data suggest that these non-physiologic IAR locations may, in turn, increase facet forces and subsequent arthritis risk.

The relationships between IAR location and facet force during compression and shear loading is also important to consider when designing disc arthroplasty devices. Since disc replacement certainly modifies the IAR, facet joint modification should be included as a critical design factor. Through a combination of joint distraction (during device implantation) and IAR optimization, these devices should be designed so as to reduce facet forces and thereby protect the joints from iatrogenic arthritis. Our data suggest that the ideal IAR path would be cephalad during flexion, posterior or caudal during extension, and laterally in bending to mimic the kinematics of the intact L5/S1 level.

Acknowledgements Our thanks are due to Spine Solutions Inc. for extending financial support.

References

1. Adams M, Hutton W (1980) The effect of posture on the role of the apophysal joints in resisting intervertebral compressive force. J Bone Joint Surg 62(B3):358–362
2. Adams M, Hutton W, Stott J (1980) The resistance to flexion of the lumbar intervertebral joint. Spine 5:245–253
3. Bertagnoli R, Kumar S (2002) Indications for full prosthetic disc arthroplasty:a correlation of clinical outcomes against a variety of indications. Eur Spine J 11(S2):131–136
4. Buttermann G, Kahmann R, Lewis J, Bradford D (1991) An experimental method for measuring force on the spinal facet joint:description and application of the method. J Biomech Bioeng 113:375–387
5. Cholewicki J, Crisco J, Oxland T, Yamamoto I, Panjabi M (1996) Effects of posture and structure on three-dimensional coupled rotations in the lumbar spine. A biomechanical analysis. Spine 21:2421–2428
6. Cripton P, Bruehlmann S, Orr T, Oxland T, Nolte L (2000) In vitro preload application during spine flexibility testing:towards reduced apparatus-related artefacts. J Biomech 33:1559–1568
7. Dunlop R, Adams M, Hutton W (1984) Disc space narrowing and the lumbar facet joints. J Bone Joint Surg 66(B5):706–710
8. Duval-Beaupere G, Robain G (1987) Visualization on full spine radiographs of the anatomical connections pf the centes of the segmental body mass supported by each vertebra and measured in vivo. Int Orthp 11:261–269
9. Gertzbein S, Holtby R, Tile M, Kapasouri A, Chan K, Cruickshank B (1984) Determination of a locus of instantaneous centers of rotation of the lumbar disc by Moiré Fringes. A new technique. Spine 9(4):409–413
10. Gertzbein SD, Chan KH, Tile M, Seligman J, Kapasouri A (1985) Moire patterns: an accurate technique for determination of the locus of the centres of rotation. J Biomech 18(7):501–509
11. Granata K, Marras W (1995) An EMG-assisted model of trunk loading during free-dynamic lifting. J Biomech 28(11):1309–1317
12. Haher T, Bergman M, O'Brien M, Felmly W, Choueka J, Welin D, Chow G, Vassiliou A (1991) The effect of the three columns of the spine on the instantaneous axis of rotation in flexion extension. Spine 16(8S):S312–S318
13. Kinzel G, Hall A, Hillberry B (1972) Measurement of the total motion between two body segments - I. Analytical development. J Biomech 5:93–105
14. Lazennec J, Ramaré S, Arafati N, Laudet C, Gorin M, Roger B, Hansen S, Sailllant G, Maurs L, Trablesi R (2000) Sagittal alignment in lumbosacral fusion: relations between radiological parameters and pain. Eur Spine J 9:47–55
15. Legaye J, Duval-Beaupere G, Hecquet J, Marty C (1998) Pelvic incidence: a fundamental parameter for three-dimensional regulation of spinal sagittal curves. Eur Spine J 7:99–103
16. Link HD (2002) History, design and biomechanics of the LINK SB Charite artificial disc. Eur Spine J 11(Suppl 2):S98–S105
17. Lorenz M, Patwardhan A, Vanderby R (1983) Load-bearing characteristics of lumbar facets in normal surgically altered spinal segments. 1982 Volvo award in biomechanics. Spine 8(2):122–130
18. Mayer H, Wiechert K, Korge A, Qose I (2002) Minimally invasive total disc replacement: surgical technique and preliminary clinical results. Eur Spine J 11(S2):124–130
19. Mc Glashen K, Miller J, Schultz A, Andersson G (1987) Load displacement behavior of the human lumbo-sacral joint. J Orthop Res 5(4):488–496
20. McGill S, Norman R (1987) Effects of an anatomically detailed erector spinae model on L4/L5 disc compression and shear. J Biomech 20(6):591–600
21. Nachemson A (1966) The load on lumbar disks in different positions of the body. Clin Orthop 45:107–122
22. Ogston N, King G, Gertzbein S, Tile M, Kapasouri A, Rubenstein J (1986) Centrode patterns in the lumbar spine. Baseline studies in normal subjects. Spine 11(6):591–595

23. Oxland T, Crisco J, Panjabi M, Yamamoto I (1992) The effect of injury on toational coupling at the lombosacral joint. A biomechanical investigation. Spine 17(1):74–80
24. Panjabi M (1979) Centers and angles of rotation of body joints: a study of errors and optimization. J Biomech 12:911–920
25. Panjabi M, Oxland T, Yamamoto I, Crisco J (1994) Mechanical behavior of the human lumbar and lumbosacral spine shown by three-dimensional load-displacement curves. J Bone Joint Surg 76(A3):413–424
26. Panjabi M, Yamamoto I, Oxland T, Crisco J (1989) How does posture affect coupling in the lumbar spine?. Spine 14(9):1002–1011
27. Pearcy M, Bogduk N (1988) Instantaneous axes of rotation of the lumbar intervertebral joints. Spine 13(9):1033–1041
28. Pearcy M, Portek I, Shepherd J (1984) Three-dimensional X-ray analysis of normal movement in the lumbar spine. Spine 9(3):294–297
29. Pearcy MJ, Tibrewal SB (1984) Axial rotation and lateral bending in the normal lumbar spine measured by three-dimensional radiography. Spine 9(6):582–587
30. Posner I, White A, Edwrds W, Hayes W (1982) A biomechanical analysis of the clinical stability of the lumbar and lumbosacral spine. Spine 7(4):374–389
31. Sakamaki T, Katoh S, Sairyo K (2002) Normal and spondylolytic pediatric spine movements with reference to instantaneous axis of rotation. Spine 27(2):141–145
32. Schendel M, Wood K, Buttermann G, Lewis J, Ogilvie J (1993) Experimental measurement of ligament force, facet force, and segment motion in the human lumbar spine. J Biomech 26(4/5):427–438
33. Schultz A, Andersson G, Ortengren R, Bjork R, Nordin M (1982) Analysis and quantitative myoelectric measurements of loads on the lumbar spine when holding weights in standing postures. Spine 7(4):390–397
34. Seligman J, Gertzbein S, Tile M, Kappasouri A (1984) Computer analysis of spinal segment motion in degenerative disc disease with and without axial loading. Spine 9(6):566–573
35. Shirazi-Adl A, Drouin G (1987) Load-bearing role of facets in a lumbar segment under sagittal plane loadings. J Biomech 20(6):601–613
36. Spoor C, Veldpaus F (1980) Rigid body motion calculated from spatial coordinates markers. J Biomech 13(4):391–393
37. Szpalski M, Gunzburg R, Mayer M (2002) Spine arthroplasty:a historical review. Eur Spine J 11(Suppl 2):S65–S84
38. Vaz G, Roussouly P, Berthonnaud E, Dimnet J (2002) Sagittal morphology and equilibrium of pelvis and spine. Eur Spine J 11(1):81–87
39. White A, Panjabi M (1990) Clinical biomechanics of the spine, 2nd edn. Lippincott Company, Philadelphia
40. Woltring H, Huiskes R, De Lange A (1985) Finite centroid and helical axis estimation from noisy landmark measurement in the study of human joint kinematics. J Biomech 18(5):379–389
41. Yamamoto I, Panjabi MM, Crisco T, Oxland T (1989) Three-dimensional movements of the whole lumbar spine and lumbosacral joint. Spine 14(11):1256–1260
42. Yamamoto I, Panjabi MM, Oxland TR, Crisco JJ (1990) The role of the iliolumbar ligament in the lumbosacral junction. Spine 15(11):1138–1141
43. Yoshioka T, Tsuji H, Hirano N, Sainoh S (1990) Motion characteristics of the normal lumbar spine in young adults: instantaneous axis of rotation and vertebral center motion analyses. J Spinal Disord 3(2):103–113